

## Leidenfrost drop dynamics: Exciting dormant modes

Jesse E. Bergen, Bailey C. Basso, and Joshua B. Bostwick <sup>\*</sup>*Department of Mechanical Engineering, Clemson University, Clemson, South Carolina 29631, USA*

(Received 16 April 2019; published 30 August 2019)

Leidenfrost drops exhibit complex shape oscillations on curved substrates. Experiments are conducted using six different liquids on three substrate geometries: curved, targeted, and toroidal, and the droplet dynamics are characterized by their oscillation amplitude. Moderate amplitude star oscillations are most common and a number of previously unreported modes are observed. Large drops exhibit constant frequency oscillations, irrespective of mode number, consistent with prior observation. Small amplitude polygonal oscillations exhibit similar dynamics to star oscillations but with twice the frequency and half the wavelength. A large amplitude  $n = 2$  dominates mode selection by suppressing higher-order modes over a large range of drop sizes in the most viscous liquids. Using the targeted substrate geometry allows for observation of those “dormant” modes. Two modes with unique oscillation frequencies can be simultaneously excited on the same drop with a frequency ratio that takes on a fixed value.

DOI: [10.1103/PhysRevFluids.4.083603](https://doi.org/10.1103/PhysRevFluids.4.083603)

### I. INTRODUCTION

A liquid drop placed on a sufficiently heated horizontal substrate experiences film boiling that generates an insulating vapor layer upon which the drop can levitate in a relatively friction-free state [1]. Here the weight of the drop is balanced by the lubrication pressure of the vapor in what is called the Leidenfrost effect [2]. The phenomenon occurs naturally in numerous heat transfer applications [3] and has been used for drag reduction [4,5] and soft engines [6]. The subject is nicely summarized in the review by Quéré [1], which discusses numerous applications and provides a comprehensive description of the physics therein.

Leidenfrost drops are subject to hydrodynamic instabilities reflecting the balance between gravity, surface tension and lubrication pressures. For example, recent studies include drop shape and vapor layer geometry [7,8], impact and spreading dynamics [9,10], and the stability of the vapor layer using micro textured surfaces [5]. Spontaneous drop translation can occur on smooth [11] and/or microstructured substrate geometries [12–15]. Of particular interest are the star oscillations first observed by Holter and Glasscock [16] and subsequently studied by many others [17–24]. Here azimuthal surface oscillations develop along the periphery of drops. Similar star-shaped oscillations have also been reported in drops levitated by air flow [25] and in microgravity [26]. Brunet and Snoeijer [27] summarizes the hydrodynamic origin of the phenomenon. There has been some dispute in the literature on the dependence of oscillation frequency on drop size  $R$ . In seminal work by Ma and Burton [24], they conduct a comprehensive experimental study of Leidenfrost star oscillations on curved substrates and show the oscillation frequency is independent of  $R$  for large drops and only depends upon the capillary length  $l_c \equiv \sqrt{\sigma/\rho g}$  [although they do observe size effects for lower order modes]. They are able to observe a large number of modes in six different liquids and reveal the source of star oscillations as pressure fluctuations in the vapor layer, which gives rise

---

\*jbostwi@clemson.edu; <https://cecas.clemson.edu/~jbostwi/>

to parametric oscillations in the drop. The independence of frequency on drop size implies that the mode number is completely determined by the drop size. This beautiful result is described in the *Focus on Fluids* article by Brunet [28]. In this paper, we build upon the results of Ma and Burton [24] by reporting previously undiscovered star oscillation modes and other complex dynamics, such as a dominant large amplitude  $n = 2$  mode and the simultaneous excitation of two unique modes at differing oscillation frequencies, both of which highlight the rich behavior in Leidenfrost drops.

Complex droplet dynamics are often associated with nonlinearities due to large amplitude deformations. These often build off the fundamental frequency  $\omega$  relationship

$$\omega^2 = \frac{n(n+2)(n-1)\sigma}{\rho R^3}, \quad (1)$$

for an inviscid liquid drop where  $\rho$  is the liquid density,  $\sigma$  the surface tension, and  $n$  the mode number of a spherical drop of radius  $R$ . These are called Rayleigh oscillations [29]. For a two-dimensional puddle, the drop is cylindrical and Eq. (1) can be modified by changing the prefactor  $n(n+2)(n-1) \rightarrow n(n-1)(n+1)$ . Nonlinear effects include the development of frequency-amplitude relationships [30], models of nonlinear modal interactions in standard [31] and electrically charged drops [32], and hysteretic phenomena [33]. Nonlinear effects are important in our experiments and we report a large amplitude  $n = 2$  mode that dominates the drop response over a large range of drop sizes where we might expect higher order modes to be excited. It was perhaps for this reason that Ma *et al.* [23] could not observe a number of star oscillation modes. We address this by using a targeted substrate geometry, which allows us to excite these previously inaccessible “dormant” modes. For free drops, the temporal response can be harmonic, as seen in superdeformed drops in microgravity [34], or subharmonic, as observed in drops in ultrasonic levitation [35], and this distinction can often provide insight into the forcing mechanism. Harmonic and subharmonic response is distinguished by the relationship between the driving frequency  $f_d$  and oscillation frequency  $f_o$ ; harmonic has  $f_d = f_o$  and subharmonic has  $2f_d = f_o$ . Ma *et al.* [23] have shown that Leidenfrost star oscillations are excited subharmonically from an oscillating pressure field in the vapor layer. In our experiments, we find that two modes can be simultaneously excited with different frequencies whose ratio is approximately four. This mode mixing behavior has been seen in previously in Faraday waves [36], star-shaped surface gravity waves [37], drop atomization [38], and in sessile drop vibrations [39,40]. The inherent advantage in Leidenfrost drops is the realization of a non-wetting condition or the absence of liquid/solid contact which is known to affect the oscillation dynamics [41,42].

We begin this paper by defining the experimental protocol to induce Leidenfrost star oscillations on curved substrates. The observed motions are characterized by their oscillation amplitude into polygons (small), stars (moderate), and large amplitude modes, and we quantify the dynamics for each and contrast our results against those recently reported [24]. Two particularly noteworthy observations include (i) a large amplitude  $n = 2$  mode that dominates the dynamic response in a regime where we expect higher order modes and (ii) the simultaneous excitation of two modes with different frequency. By using a targeted substrate geometry we are able to realize a number of previously undiscovered or inaccessible modes. Lastly, some concluding remarks are offered.

## II. EXPERIMENT

Experiments are performed on substrates which confine drops to a prescribed geometry and are constructed from either 360 brass or 6061 aluminum, as shown in Fig. 1. A hotplate controls the substrate temperature up to 723 K, which is measured by a thermocouple, and the substrate is leveled to within  $0.1^\circ$ . We use six liquids in our study: distilled water, acetone, isopropyl alcohol, methanol, ethanol (denatured), and liquid nitrogen, whose liquid properties at boiling temperature are given in Table I [43]. Typical substrate temperatures during experiment ranged from 473 K to 673 K, with the exception of liquid nitrogen which did not need substrate heating due to the low boiling temperature. In general, and with the exception of liquid nitrogen, we tended to observe the

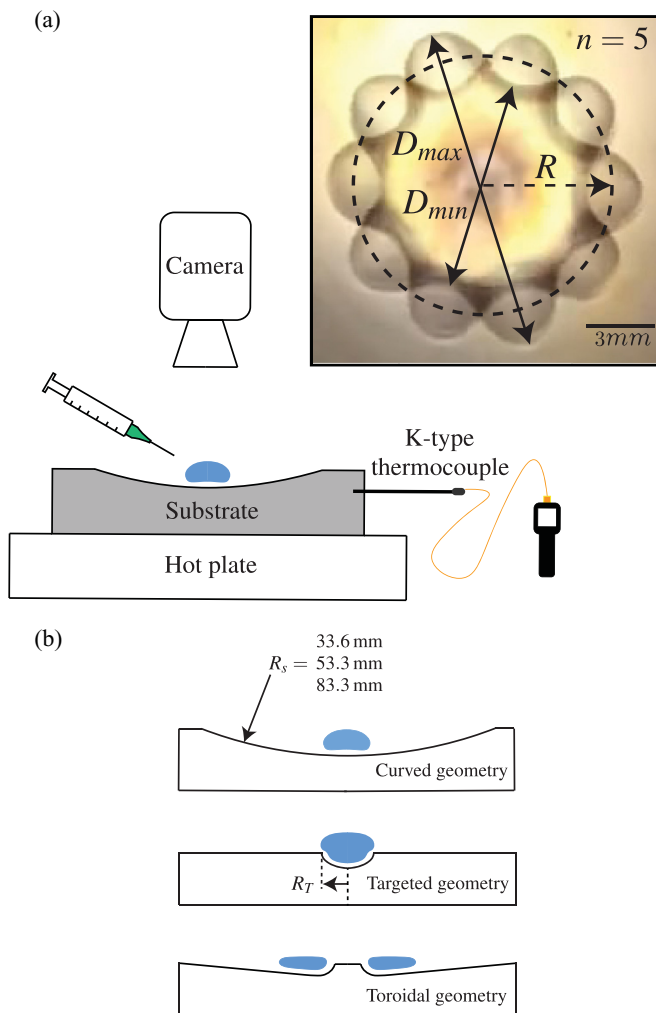


FIG. 1. (a) Schematic of experimental setup and image processing technique (inset) illustrating how the equilibrium radius  $R$  and surface disturbance amplitude  $(D_{\max} - D_{\min})/2$  are determined and (b) the three substrate geometries used in experiment; curved, targeted and toroidal.

TABLE I. Liquid properties at the respective boiling temperature: density  $\rho$  [ $\text{kg m}^{-3}$ ], surface tension  $\sigma$  [ $\text{mN m}^{-1}$ ], viscosity  $\eta$  [ $\text{mPa s}$ ], capillary length  $l_c$  [ $\text{mm}$ ], and boiling temperature  $T_B$  [ $\text{K}$ ] taken from Lemmon *et al.* [43].

Liquid	$\rho$	$\sigma$	$\eta$	$l_c$	$T_B$
Water	958	59.0	0.282	2.5	373
Acetone	727	18.2	0.242	1.6	329
Isopropanol	723	15.7	0.460	1.5	356
Methanol	748	18.9	0.295	1.6	338
Ethanol	750	18.6	0.420	1.6	352
Liquid Nitrogen	807	8.90	0.162	1.1	77

low order  $n = 2-4$  modes at our highest surface temperature 673 K and the high order  $n > 4$  modes at reduced surface temperatures 473 K to 573 K. We note that no substrate heating was required for liquid nitrogen to due to its low Leidenfrost temperature.

We begin each experiment by heating the substrate above the Leidenfrost temperature and then depositing a volume of liquid on the substrate using a syringe. The drop then spontaneously begins to oscillate about its equilibrium shape. This instability appears along the periphery of the drop in the form of azimuthal surface oscillations giving the drop the appearance of a star with a fixed number of outer lobes or vertices. Hereafter, we will refer to this instability as Leidenfrost star oscillations. Most oscillations typically took from several seconds up to a minute to fully develop (i.e., transients to decay) and were self-sustained displaying over 50 periods of oscillation at minimum. Videos are captured using a Phantom VEO 410L high speed camera at 3900 fps with  $1280 \times 800$  px resolution from above the substrate and analyzed to measure the frequency of oscillation  $f$ , equilibrium drop radius  $R$  (equivalently, volume), and mode number  $n$  for each oscillating drop. The frequency  $f$  is measured by dividing the frame-rate of the camera by the number of frames taken to complete one cycle of oscillation. To measure the equilibrium radius  $R$ , we overlay two images of a drop during oscillation, one at maximal extension and another one-half period out of phase with respect to the first, as shown in Fig. 1(a) (inset). This combined image is imported into NIH ImageJ software for processing. This method can also be used to calculate the scaled oscillation amplitude  $\epsilon = (D_{\max}/2 - R)/R$ . Mode number  $n$  is determined by counting the number of vertices along the circumference of the drop.

The surface geometry of the substrate is of principle interest in this study. Figure 1(b) shows a schematic of our three substrate geometries; curved, targeted, and toroidal. For the majority of our experiments, we use the curved geometry common to other experimental studies of Leidenfrost star oscillations [23,25]. The curved substrate takes the shape of a shallow bowl with three different radii-of-curvature  $R_s = 33.6$  mm, 53.3 mm, or 83.3 mm and constrains the drop to lie at the bottom of the bowl. Experiments on the curved substrates yield the majority of our data; however, it was necessary to fabricate two alternative geometries in order to observe select modes that did not appear on the curved substrate. The first is called the targeted geometry and is constructed from a flat plate with a hemispherical depression of fixed radius  $R_T$ . A number of such plates were used to isolate drops of a prescribed size  $R_T$ . The second is a toroidal geometry that confines liquid to a toroidal drop configuration.

### III. RESULTS

We report experimental observations of three unique regimes of oscillation for a fixed mode number and a complex drop motion that involves the nondestructive superposition of two modes of different frequencies, which we call modal coexistence. These are all capillary oscillations. We distinguish the three oscillations types by their amplitude  $\epsilon$ , small (polygons), moderate (stars), and large amplitude. The majority of our observations lie in the moderate amplitude star oscillation regime and we report a number of previously unreported modes [24]. Large amplitude  $n = 2$  modes are shown to dominate the dynamics over a range of parameters where one would expect higher order modes to appear. We “fill out” or complete our data set by using alternative substrate geometries, targeted and toroidal, which are able to excite modes which did not appear on our typical curved substrates. Finally, we report observations of mode mixing where two modes of oscillation coexist simultaneously in synchronized resonance.

#### A. Star oscillations

The most common instability we observe on the curved substrate geometry is the star oscillation pattern, shown in Fig. 2 for water drops with mode number  $n = 2-15$ , consistent with Ma *et al.* [23]. Note that the relative size of each drop is preserved in the images for  $n = 2-13$  and the mode number  $n$  increases with drop radius  $R$ . Otherwise stated, the mode number  $n$  is essentially set by



FIG. 2. Experimentally observed star oscillations in water drops with mode numbers  $n = 2$ –15 on  $R_s = 83.3$  mm plate.

the circumference of the drop; however this is not always the case as Fig. 2 clearly shows an  $n = 5$  drop which is larger than the  $n = 6$  drop. In general, we observe that (i) a given mode  $n$  can be excited over a range of  $R$  and (ii) there are a number of modes  $n$  that exist for a given  $R$ . For some liquids (ethanol, methanol, isopropanol), the range of  $R$  can be large and in this region there is a dominant mode that suppresses the observation of other modes. We discuss this phenomena in a later section.

Figure 3 presents our experimental data set for the curved and targeted substrate geometries and plots the drop oscillation frequency  $f$  in Hertz against scaled radius  $R/l_c$  for the six liquids, where  $l_c$  is the capillary length of the respective liquid. We observe Leidenfrost drop oscillations with frequencies ranging from  $f = 3$ –84 Hz, drop size from  $R/l_c = 1$ –10 and mode number from  $n = 2$ –15. For small drops, the frequency  $f$  varies significantly with drop size  $R/l_c$ , as indicated by the scatter in  $f$  at small  $R/l_c$ . One striking feature of Fig. 3 is the appearance of nearly constant  $f$  for large drops (defined as approximately  $R/l_c > 4$ ), consistent with Ma *et al.* [23], Ma and Burton [24]. At this point, we note that we have observed modes  $n = 2$ –15 for water,  $n = 2$ –11 for acetone,  $n = 2, 3, 6$ –12 for isopropanol and ethanol,  $n = 2, 3, 5$ –12 for methanol, and  $n = 2$ –9 for liquid nitrogen, on the curved geometry, which encompass those modes observed by Ma *et al.* [23] and

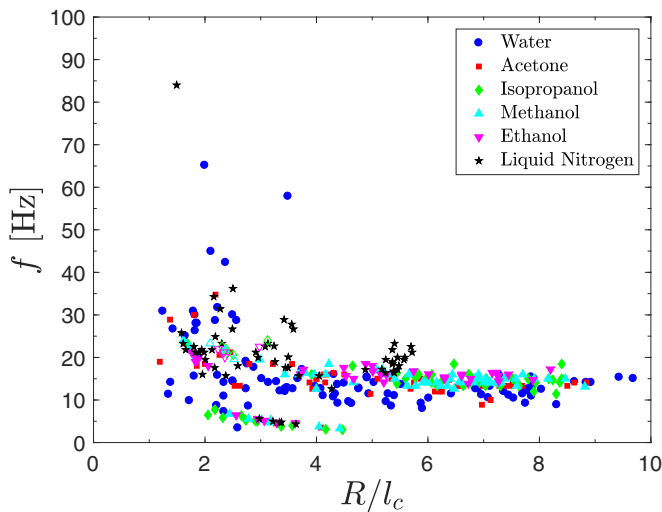


FIG. 3. Oscillation frequency  $f$  [Hz] against scaled radius  $R/l_c$  sorted by liquid. Solid symbols denote the curved geometry and open symbols the targeted geometry.

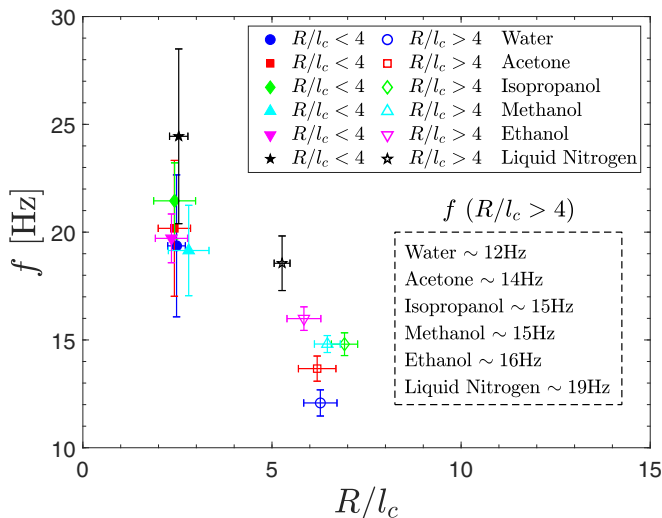


FIG. 4. Frequency  $f$  [Hz] against drop size  $R/l_c$  shows strong size dependence for small  $R < 4l_c$  drops, while large drops  $R > 4l_c$  oscillate with constant frequency (inset). Error bars are 95% confidence intervals.

many others. The  $R_s = 33.6$  mm plate was used for liquid nitrogen,  $R_s = 53.3$  mm for acetone, ethanol, methanol and isopropanol, and  $R_s = 83.3$  mm for water. To observe the missing modes and complete our data set, we use a different substrate geometry which we discuss in a subsequent section.

There has been some disagreement in the literature on whether Leidenfrost star oscillation frequency  $f$  depends on drop radius  $R$  [22–24,28,44,45] and we clarify this dependence by sorting our complete data set, shown in Fig. 3, into two regimes based on drop size  $R/l_c$ . The statistics of this sorting are presented in Fig. 4 which shows how frequency  $f$  is affected by  $R/l_c$  for small  $R/l_c < 4$  and large  $R/l_c > 4$  drops. Small drops have strong size dependence as indicated by the relatively large 95% confidence intervals in  $f$  (vertical error bar), while large drops have a constant frequency for each liquid that is independent of size  $R/l_c$  and mode number  $n$ . The constant oscillation frequency for each liquid is shown in the dashed inset of Fig. 4. We only realize constant  $f$  for large oscillating Leidenfrost drops with  $R/l_c > 4$ .

For large drops, the mode number  $n$  is essentially set by the drop size  $R/l_c$ . Figure 5 plots mode number  $n$  against drop radius  $R$  for each liquid, where circles and stars denote drops on curved and targeted substrate geometries, respectively. Each liquid displays an approximately linear trend  $n \sim R$  with the scatter highlighting unique behavior for each liquid. For fixed frequency, this scaling is consistent with Eq. (1), i.e., constant  $\omega$  implies  $n(n+2)(n-1)\sigma/\rho R^3$  is also constant, up to a pre-factor that could be related to the flattening of the drop due to gravity, viscous or finite amplitude effects, or some combination thereof. Water, acetone and liquid nitrogen show a larger variation in  $R$  for a given mode number  $n$ , while isopropanol, methanol and ethanol display a tighter tolerance in  $R$  for a given  $n$ . With regards to the latter, each mode number  $n$  depends sensitively on a narrow range of  $R$  with the exception of the  $n = 2$  mode which exists over a large range of  $R$ . We discuss the unique dynamics of this special mode in subsequent sections. Overall, we believe liquid viscosity plays a role in mode selection with higher viscosity liquids limiting the range of  $R$  in which a given mode  $n$  may exist, consistent with Ma and Burton [[24], cf. Fig. 10].

### 1. Targeted modes

We were able to excite nearly all modes on the curved substrate geometry, as shown in Fig. 5 (black circles) which plots mode number  $n$  against drop radius  $R$  for all liquids. However, we could

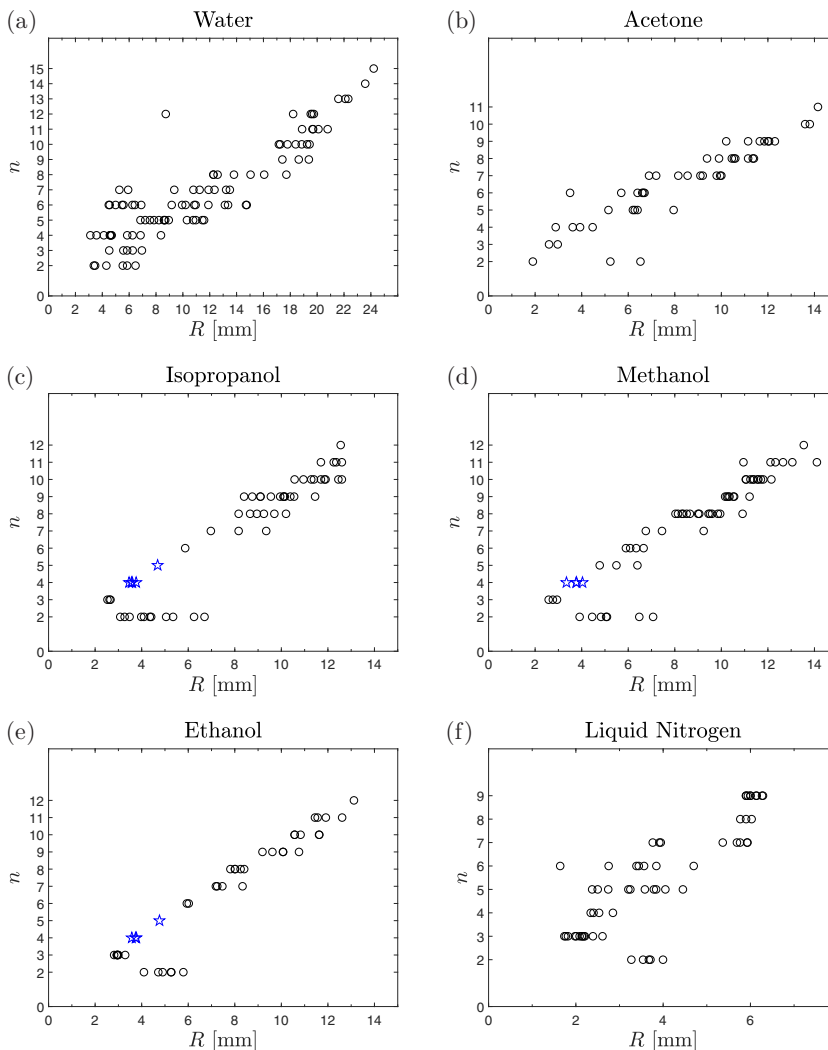


FIG. 5. Mode number  $n$  against radius  $R$  for (a) water, (b) acetone, (c) isopropanol, (d) methanol, (e) ethanol, and (f) liquid nitrogen. Star symbols denote observations on the targeted substrate geometry.

not observe the  $n = 4, 5$  modes for isopropanol and ethanol and the  $n = 4$  mode for methanol on the curved geometry. Figure 5 reveals a linear trend between mode number and radius, and the missing modes have radius  $R$  that lies between the  $n = 3$  and  $n = 6$  modes for isopropanol and ethanol and between the  $n = 3$  and  $n = 5$  modes for methanol. Over this range of  $R$  we observe a large amplitude  $n = 2$  mode that dominates the droplet response, as shown in Figs. 5(c)–5(e) for isopropanol, methanol, and ethanol, respectively. Note the large range of radius where this mode can be excited. In an effort to excite modes other than  $n = 2$  in this range, we constructed a targeted substrate geometry consisting of a shallow hemispherical depression of radius  $R_T = 2.35$  mm and depth  $d = 1.3$  mm machined into a flat plate. The radius  $R_T$  was specifically chosen to lie within the expected range of  $R$  for the missing modes, as determined directly from Fig. 5. Using the targeted geometry, we were able to observe the missing modes, indicated by blue stars in Fig. 5, and complete our data set. However, these oscillations were generally more disordered than typical star oscillations which we attribute to the dominance of the  $n = 2$  mode in this regime. In a subsequent section we further discuss the dynamics of the large amplitude  $n = 2$  modes.



FIG. 6. Drop oscillations exhibit mode numbers  $n = 15$ – $17$  on the toroidal geometry using water.

## 2. Toroidal substrate geometry

Leidenfrost star oscillations can also be excited on the toroidal substrate geometry shown in Fig. 1(b). The geometry is similar to that used by Perrard *et al.* [46], who observed rotating surface instabilities on the interior radius of toroidal drops. However, in contrast to Perrard, we purposefully fabricated the geometry to excite surface instabilities along the outer radius of a toroidal liquid drop. Rather than the expected rotating polygonal structure, we observe typical moderate amplitude star oscillations along the outer circumference of the liquid ring with mode numbers  $n = 15$ – $17$ , as shown in Fig. 6. The frequency  $f$  of these toroidal drops is found to be consistent with that of drops larger than  $R/l_c > 4$  on the curved geometries. This observation leads us to believe star oscillations originate from, and are localized near, the outer edge of the drop, and that the fluid dynamics in the center of the drop play little role in the instability. The fact that we are able to excite higher mode numbers using the toroidal geometry is related to the ability to create large radius drops, consistent with our observations (cf. Fig. 5). Furthermore, the toroidal geometry may play some role in suppressing the chimney instability our largest drops [7].

## B. Polygonal oscillations

Oscillating Leidenfrost drops did not always assume the shape of a star. Often times, drops were observed to undergo the small amplitude oscillations shown in Fig. 7. These shapes are polygonal with well-defined sides and discrete vertices. Observations in this regime were generally limited to water, although acetone and liquid nitrogen did exhibit similar behavior. These small amplitude oscillations are characterized by a radius (equivalently, wavelength) approximately half that of typical star oscillations and frequency  $f$  approximately twice that; however, much higher frequencies were also observed, e.g., the high frequency  $f \approx 65$ – $85$  Hz,  $n = 6$  modes in Fig. 9 are polygonal modes. This suggests the mode selection mechanism is more complicated for smaller drops. A possible explanation would be that the polygonal modes exhibit a harmonic response with respect to the pressure field in the vapor layer, as opposed to the subharmonic response for star oscillations [23,24]. However, we did not monitor the pressure field in our experiments and therefore can not corroborate this hypothesis. These motions were difficult to detect in experiment due to the small oscillation amplitude.

Figure 8 plots mode number  $n$  against radius  $R$  for water. Two distinct linear trends  $n \sim R$  emerge; the first trend (denoted by the solid line) corresponds to our typical moderate amplitude star oscillations, while the second trend (dashed line) represents our small amplitude polygonal

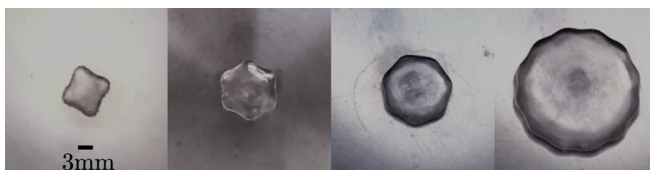


FIG. 7. Typical polygonal modes with  $n = 4, 6, 7, 12$  using water.

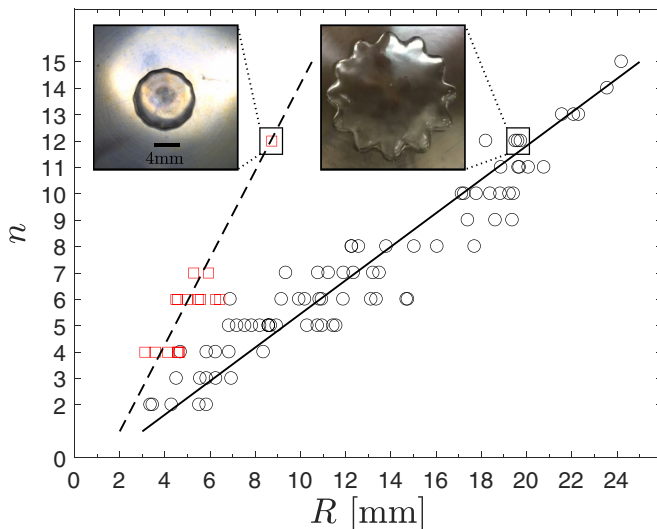


FIG. 8. Mode number  $n$  against drop radius  $R$  for water drops on  $R_s = 83.3$  mm curved substrate exhibits star oscillations (circles, solid line type) and polygonal modes (squares, dashed line type).

oscillations. For a given  $n$ , we clearly show the polygonal oscillations are approximately half the radius  $R$  of star oscillations (cf. Fig. 8 insets contrasts the  $n = 12$  modes in the polygonal and star regimes). These distinct trend lines allows one to clearly define the difference between star and polygonal modes, e.g., the  $n = 4$  mode shown in Fig. 7 may appear visually to be a star mode but lies along the polygonal mode trend line and is therefore identified as such. Based on the number of observations of each mode number, we see the polygonal oscillation is most prevalent in the  $n = 4$  and  $n = 6$  mode shapes. Figure 8 shows that polygonal modes exist over a range of radius  $R$  where a lower mode number star oscillation is expected. Accordingly, the fact that polygonal oscillations are only observed in our least viscous liquids suggests that viscosity plays a role in star vs. polygonal mode selection, i.e., there is a competition between mode number  $n$  and oscillation amplitude  $\epsilon$  that occurs in viscous dissipation.

### C. Large amplitude $n = 2$ modes

Figure 9 presents our data set sorted by mode number  $n$  and illustrates that the  $n = 2$  modes are fundamentally different than the typical star oscillations discussed above. These drops are characterized by a larger-than-expected drop size  $R/l_c$  (the  $n = 3$  modes are generally smaller in size than the  $n = 2$  modes), low frequency  $f$ , and much larger amplitude, in comparison to typical star oscillations. Qualitatively, the  $n = 2$  modes take the shape of a flattened spheroid, as shown in Fig. 10 (inset). Figure 9 shows that typical star oscillations with mode number  $n \gtrsim 8$  have constant frequency  $f$  such that drop size  $R/l_c$  is an effective metric to realize constant frequency oscillations.

Observations of large amplitude oscillations are generally limited to  $n = 2$ , with the exception of mode doubling phenomena which will be discussed shortly. When compared to moderate amplitude star oscillations, the  $n = 2$  modes have approximately twice the radius (equivalently, wavelength) and half the frequency, and significantly larger oscillation amplitude  $\epsilon$ . This dominant  $n = 2$  mode of oscillation is observed in all liquids, but is most prevalent in liquids other than water. We believe viscosity to play a role in damping polygonal and star oscillations (higher mode numbers have larger viscous dissipation) [44], which allows the large amplitude  $n = 2$  oscillations to control the dynamics. This would account for the large number of observations of this  $n = 2$  mode in our higher viscosity liquids (cf. Fig. 5). In addition, nonlinear effects due to large oscillation amplitude

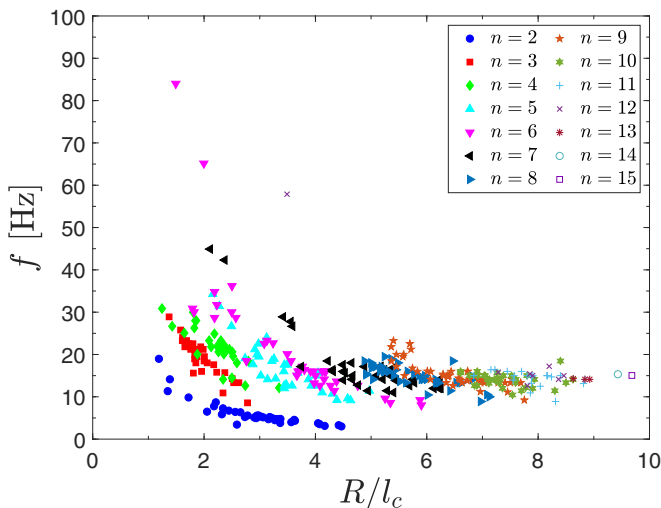


FIG. 9. Oscillation frequency  $f$  [Hz] plotted against scaled radius  $R/l_c$  sorted by mode number  $n$ .

could also explain the large range of radii (relative to other mode numbers) over which the  $n = 2$  mode is excited, as illustrated in Figs. 5(c)–5(f).

Droplet oscillation frequency is known to decrease for increasing amplitude in experiments [26]. In our experiments, the large  $n = 2$  oscillations have both lower frequency  $f$  and larger amplitude  $\epsilon$  than the typical moderate amplitude star oscillations. We measure  $\epsilon$  as large as  $\epsilon = 0.5$  for the  $n = 2$  modes and  $\epsilon \lesssim 0.1$  for typical star oscillations. Linear theory is known to breakdown at large amplitude and we use the model of Tsamopoulos and Brown [30] for the resonance frequency of a spherical drop undergoing moderate amplitude oscillations. For the  $n = 2$  mode, the frequency is given by

$$f_T = \frac{1}{2\pi} \left[ \frac{\sigma n(n-1)(n+2)}{\rho R^3} \right]^{1/2} (1 - 1.27752\epsilon^2). \quad (2)$$

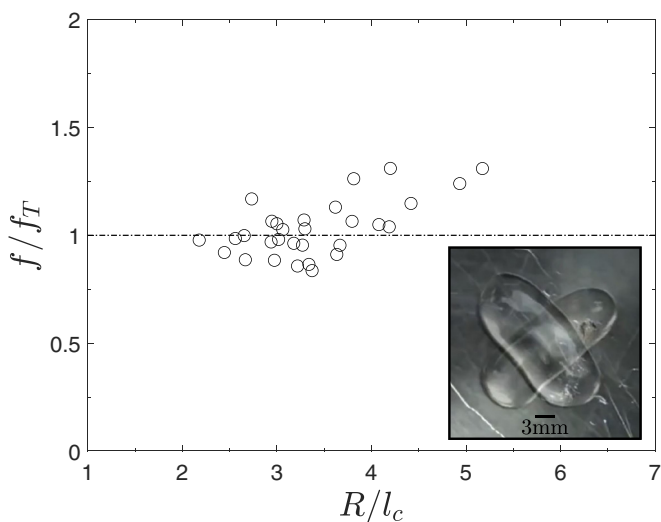


FIG. 10. Scaled frequency  $f/f_T$  against  $R/l_c$  for the large amplitude  $n = 2$  star oscillations (inset, using water).

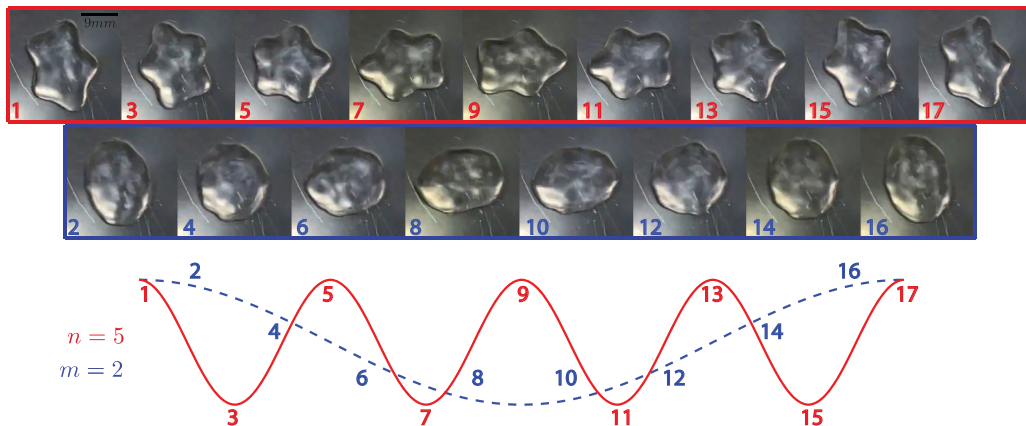


FIG. 11. Star oscillations in a water drop on  $R_s = 83.3$  mm plate exhibits the simultaneous superposition of two modes  $n = 5$  and  $m = 2$  with different frequencies. The  $n = 5$  mode completes 4 oscillation cycles within the time the  $n = 2$  mode completes 1 cycle.

Note that Eq. (2) recovers Eq. (1) when  $\epsilon = 0$ . Figure 10 plots the frequency  $f$  scaled by  $f_T$  [Eq. (2)] against scaled radius  $R/l_c$  for the  $n = 2$  modes. The agreement is good as indicated by the collapse of the data to  $f/f_T = 1$ .

#### D. Modal coexistence

Leidenfrost drops are not limited to a single mode of oscillation. Remarkably, two distinct modes are observed to coexist in stable synchronized resonance with two distinct oscillation frequencies. This phenomenon has previously been reported in experiments of vertically vibrated sessile drops, where one mode is excited harmonically and the other subharmonically with respect to the driving frequency [39,40]. Figure 11 shows a water drop that exhibits mixing between the  $n = 5$  and  $m = 2$  modes, where the high-frequency  $n = 5$  mode is shown in the upper row (red) and the low frequency  $m = 2$  mode is shown in the lower row (blue). Here the frequency of the  $n = 5$  mode is approximately 4 times that of the  $m = 2$  mode, or the  $n = 5$  mode completes 4 cycles for every 1  $m = 2$  cycle, as shown in Fig. 11 [47]. Remarkably, we observed modal coexistence in nearly all of our liquids with frequency ratio  $f_n/f_m \approx 4$  for all observations. Table II summarizes our results. In

TABLE II. Observations of modal coexistence with mode number  $n, m$  and corresponding frequency  $f_n, f_m$ .

Liquid	$n-m$	$f_n$ [Hz]	$f_m$ [Hz]	$f_n/f_m$
Water	5-2	15.33	3.93	3.90
	5-2	13.59	3.67	3.70
	6-2	14.12	3.38	4.18
Isopropanol	6-2	17.58	4.06	4.33
	7-2	17.58	3.88	4.53
Methanol	11-3	13.36	3.29	4.06
Ethanol	11-3	16.76	4.51	3.72
	11-3	17.14	4.92	3.49
	12-3	17.14	3.88	4.42
Liquid Nitrogen	6-2	30.00	6.41	4.68

general, mode mixing occurs between a typical star oscillation with mode number  $n$  that is localized on the drop periphery and a low frequency shape modulation of the drop shape with mode number  $m$ . Shape modulation has been observed for  $m = 2-4$ , where  $m = 2$  corresponds to an oval,  $m = 3$  a triangle, and  $m = 4$  a square. Here the  $m$  modes are reminiscent of the large amplitude  $n = 2$  mode discussed in the previous section. It is possible that the excitation mechanism is identical to that of star oscillations where the vapor pressure field has a single frequency but can excite two modes simultaneously, one harmonically and the other subharmonically. However, this is speculation since we did not measure vapor pressure dynamics.

#### IV. CONCLUDING REMARKS

We have reported experimental observations of complex dynamics in oscillating Leidenfrost drops, which we categorize by oscillation amplitude into three distinct regimes; small, moderate, and large. Moderate amplitude star oscillations are the most common observed motions and our results extend the seminal work by Ma *et al.* [23], Ma and Burton [24] through the observation of many undiscovered modes, which we find either on the standard curved substrate or by using a targeted substrate geometry. We attribute the lack of prior observation to a dominant large amplitude  $n = 2$  mode that controls the dynamics for our most viscous fluids: isopropanol, ethanol, and methanol. This special motion agrees well with a large amplitude theory of Tsamopoulos and Brown [30] and persists over a large range of droplet sizes where we would expect to observe those undiscovered modes. By constructing a targeted substrate geometry, we are able to suppress that dominant mode and observe those “dormant” modes by constraining the drop to lie within a prescribed radius where we expect those modes to be excited. The size of this geometry was guided by our understanding of mode selection in star oscillations. Small amplitude polygonal oscillations are observed to have twice the frequency and half the size of typical star oscillations. Last, we have shown that two modes can be simultaneously excited on the same Leidenfrost drop and the ratio of their frequencies is approximately four.

Our work has revealed a number of new dynamic behaviors in Leidenfrost drops that should be explored further. Future directions include model development to study the physics involved in modal interactions that lead to the dominant  $n = 2$  behavior for viscous fluids and the resonance conditions that give rise to the complex modal mixing phenomenon we observe. Ma and Burton [24] has revealed the instability mechanism for star oscillations to be related to the pressure field in the vapor layer generated from evaporation and, therefore, hydrodynamic in nature. They postulate that a sufficiently large shear stress at the liquid/gas interface due to the escaping vapor can generate capillary waves that travel from the center of the drop to the periphery and that this excites star oscillations. Of course the magnitude of this shear stress is indirectly related to the evaporative heat transfer beneath the drop which may play a role in defining the critical bifurcation parameter for this instability. The role of hydrodynamics in the star oscillation instability leads one to believe that the aforementioned behaviors could be understood solely through the capillary dynamics of liquid drops, as exhibited by the collapse of the large amplitude  $n = 2$  modes to a nonlinear theory of drop oscillations (cf. Fig. 10).

#### ACKNOWLEDGMENT

We acknowledge support from the Clemson University Creative Inquiry program.

---

[1] D. Quéré, Leidenfrost dynamics, *Annu. Rev. Fluid Mech.* **45**, 197 (2013).

[2] J. G. Leidenfrost, *De aquae communis nonnullis qualitatibus tractatus* (Ovenius, Duisburg, Germany, 1756).

- [3] H. Van Dam, Physics of nuclear reactor safety, *Rep. Prog. Phys.* **55**, 2025 (1992).
- [4] I. U. Vakarelski, J. O. Marston, D. Y. C. Chan, and S. T. Thoroddsen, Drag Reduction by Leidenfrost Vapor Layers, *Phys. Rev. Lett.* **106**, 214501 (2011).
- [5] I. U. Vakarelski, N. A. Patankar, J. O. Marston, D. Y. C. Chan, and S. T. Thoroddsen, Stabilization of Leidenfrost vapour layer by textured superhydrophobic surfaces, *Nature* **489**, 274 (2012).
- [6] S. R. Waitukaitis, A. Zuiderwijk, A. Souslov, C. Coullais, and M. Van Hecke, Coupling the Leidenfrost effect and elastic deformations to power sustained bouncing, *Nat. Phys.* **13**, 1095 (2017).
- [7] A.-L. Biance, C. Clanet, and D. Quéré, Leidenfrost drops, *Phys. Fluids* **15**, 1632 (2003).
- [8] J. C. Burton, A. L. Sharpe, R. C. A. Van Der Veen, A. Franco, and S. R. Nagel, Geometry of the Vapor Layer Under a Leidenfrost Drop, *Phys. Rev. Lett.* **109**, 074301 (2012).
- [9] J. D. Bernardin, C. J. Stebbins, and I. Mudawar, Mapping of impact and heat transfer regimes of water drops impinging on a polished surface, *Int. J. Heat Mass Transfer* **40**, 247 (1997).
- [10] T. Tran, H. J. J. Staat, A. Prosperetti, C. Sun, and D. Lohse, Drop Impact on Superheated Surfaces, *Phys. Rev. Lett.* **108**, 036101 (2012).
- [11] A. Bouillant, T. Mouterde, P. Bourriane, A. Lagarde, C. Clanet, and D. Quéré, Leidenfrost wheels, *Nat. Phys.* **14**, 1188 (2018).
- [12] H. Linke, B. J. Alemán, L. D. Melling, M. J. Taormina, M. J. Francis, C. C. Dow-Hygelund, V. Narayanan, R. P. Taylor, and A. Stout, Self-Propelled Leidenfrost Droplets, *Phys. Rev. Lett.* **96**, 154502 (2006).
- [13] G. Lagubeau, M. Le Merrer, C. Clanet, and D. Quéré, Leidenfrost on a ratchet, *Nat. Phys.* **7**, 395 (2011).
- [14] G. Dupeux, M. Le Merrer, C. Clanet, and D. Quéré, Trapping Leidenfrost drops with crenelations, *Phys. Rev. Lett.* **107**, 114503 (2011).
- [15] D. Soto, G. Lagubeau, C. Clanet, and D. Quéré, Surfing on a herringbone, *Phys. Rev. Fluids* **1**, 013902 (2016).
- [16] N. J. Holter and W. R. Glasscock, Vibrations of evaporating liquid drops, *J. Acoust. Soc. Am.* **24**, 682 (1952).
- [17] L. H. J. Wachters, H. Bonne, and H. J. Van Nouhuis, The heat transfer from a hot horizontal plate to sessile water drops in the spheroidal state, *Chem. Eng. Sci.* **21**, 923 (1966).
- [18] K. Adachi and R. Takaki, Vibration of a flattened drop: I. Observation, *J. Phys. Soc. Jpn.* **53**, 4184 (1984).
- [19] R. Takaki and K. Adachi, Vibration of a flattened drop: II. Normal mode analysis, *J. Phys. Soc. Jpn.* **54**, 2462 (1985).
- [20] N. Tokugawa and R. Takaki, Mechanism of self-induced vibration of a liquid drop based on the surface tension fluctuation, *J. Phys. Soc. Jpn.* **63**, 1758 (1994).
- [21] D. E. Strier, A. A. Duarte, H. Ferrari, and G. B. Mindlin, Nitrogen stars: Morphogenesis of a liquid drop, *Physica A: Stat. Mech. Appl.* **283**, 261 (2000).
- [22] A. Snezhko, E. B. Jacob, and I. S. Aranson, Pulsating–gliding transition in the dynamics of levitating liquid nitrogen droplets, *New J. Phys.* **10**, 043034 (2008).
- [23] X. Ma, J.-J. Liétor-Santos, and J. C. Burton, Star-shaped oscillations of Leidenfrost drops, *Phys. Rev. Fluids* **2**, 031602 (2017).
- [24] X. Ma and J. C. Burton, Self-organized oscillations of Leidenfrost drops, *J. Fluid Mech.* **846**, 263 (2018).
- [25] J. H. Snoeijer, P. Brunet, and J. Eggers, Maximum size of drops levitated by an air cushion, *Phys. Rev. E* **79**, 036307 (2009).
- [26] T. G. Wang, A. V. Anilkumar, and C. P. Lee, Oscillations of liquid drops: Results from USML-1 experiments in space, *J. Fluid Mech.* **308**, 1 (1996).
- [27] P. Brunet and J. H. Snoeijer, Star-drops formed by periodic excitation and on an air cushion—A short review, *Eur. Phys. J.: Spec. Top.* **192**, 207 (2011).
- [28] P. Brunet, The crackling sound of Leidenfrost stars, *J. Fluid Mech.* **850**, 1 (2018).
- [29] L. Rayleigh, On the capillary phenomena of jets, *Proc. R. Soc. London* **29**, 71 (1879).
- [30] J. A. Tsamopoulos and R. A. Brown, Nonlinear oscillations of inviscid drops and bubbles, *J. Fluid Mech.* **127**, 519 (1983).
- [31] R. Natarajan and R. A. Brown, Third-order resonance effects and the nonlinear stability of drop oscillations, *J. Fluid Mech.* **183**, 95 (1987).

- [32] A. N. Zharov, A. I. Grigor'ev, and S. O. Shiryayeva, Internal nonlinear four-mode interactions of capillary oscillations of a charged drop, *Tech. Phys. Lett.* **29**, 388 (2003).
- [33] D. W. DePaoli, J. Q. Feng, O. A. Basaran, and T. C. Scott, Hysteresis in forced oscillations of pendant drops, *Phys. Fluids* **7**, 1181 (1995).
- [34] R. E. Apfel, Y. Tian, J. Jankovsky, T. Shi, X. Chen, R. G. Holt, E. Trinh, A. Croonquist, K. C. Thornton, A. Sacco, Jr., *et al.*, Free Oscillations and Surfactant Studies of Superdeformed Drops in Microgravity, *Phys. Rev. Lett.* **78**, 1912 (1997).
- [35] C. L. Shen, W. J. Xie, and B. Wei, Parametrically excited sectorial oscillation of liquid drops floating in ultrasound, *Phys. Rev. E* **81**, 046305 (2010).
- [36] W. Batson, F. Zoueshtiagh, and R. Narayanan, The faraday threshold in small cylinders and the sidewall non-ideality, *J. Fluid Mech.* **729**, 496 (2013).
- [37] J. Rajchenbach, D. Clamond, and A. Leroux, Observation of Star-Shaped Surface Gravity Waves, *Phys. Rev. Lett.* **110**, 094502 (2013).
- [38] B. Vukasinovic, M. K. Smith, and A. Glezer, Dynamics of a sessile drop in forced vibration, *J. Fluid Mech.* **587**, 395 (2007).
- [39] C.-T. Chang, J. B. Bostwick, P. H. Steen, and S. Daniel, Substrate constraint modifies the Rayleigh spectrum of vibrating sessile drops, *Phys. Rev. E* **88**, 023015 (2013).
- [40] C.-T. Chang, J. B. Bostwick, S. Daniel, and P. H. Steen, Dynamics of sessile drops: Part 2. Experiment, *J. Fluid Mech.* **768**, 442 (2015).
- [41] J. B. Bostwick and P. H. Steen, Capillary oscillations of a constrained liquid drop, *Phys. Fluids* **21**, 032108 (2009).
- [42] J. B. Bostwick and P. H. Steen, Stability of constrained capillary surfaces, *Annu. Rev. Fluid Mech.* **47**, 539 (2015).
- [43] E. W. Lemmon, M. O. McLinden, D. G. Friend, P. Linstrom, and W. Mallard, *NIST Chemistry Webbook, NIST Standard Reference Database Number 69* (National Institute of Standards and Technology, Gaithersburg, MD, 2011).
- [44] W. Bouwhuis, K. G. Winkels, I. R. Peters, P. Brunet, D. Van Der Meer, and J. H. Snoeijer, Oscillating and star-shaped drops levitated by an airflow, *Phys. Rev. E* **88**, 023017 (2013).
- [45] T. A. Caswell, Dynamics of the vapor layer below a Leidenfrost drop, *Phys. Rev. E* **90**, 013014 (2014).
- [46] S. Perrard, Y. Couder, E. Fort, and L. Limat, Leidenfrost levitated liquid tori, *Europhys. Lett.* **100**, 54006 (2012).
- [47] See Supplemental Material at <http://link.aps.org/supplemental/10.1103/PhysRevFluids.4.083603> for a video of the oscillation motion shown in Fig. 11.